Journal of Nuclear Materials 545 (2021) 152613

Contents lists available at ScienceDirect

Journal of Nuclear Materials

journal homepage: www.elsevier.com/locate/jnucmat

Recrystallization suppression through dispersion-strengthening of tungsten

E. Lang[a,*], H. Schamis[b], N. Madden[c], C. Smith[c], R. Kolasinski[d], J. Krogstad[c], J.P. Allain[b]

[a] Department of Nuclear, Plasma, and Radiological Engineering, University of Illinois at Urbana-Champaign, Urbana, IL, United States
[b] Ken and Mary Alice Lindquist Department of Nuclear Engineering, Pennsylvania State University, State College, PA, United States
[c] Materials Science and Engineering Department, University of Illinois at Urbana-Champaign, Urbana, IL, United States
[d] Sandia National Laboratories - Livermore, Plasma and Reacting Flow Science, Livermore, CA, United States

ARTICLE INFO

Article history:
Received 6 August 2020
Revised 11 October 2020
Accepted 16 October 2020
Available online 4 November 2020

Keywords:
Dispersion-strengthened tungsten
recrystallization
tungsten
nuclear fusion

ABSTRACT

Tungsten is the material of choice for the divertor region of future nuclear fusion reactors, an environment that will expose plasma-facing components (e.g. divertor, etc...) to high temperatures and transient high heat flux events. Under these conditions, recrystallization and grain growth of tungsten can occur, leading to undesirable microstructural and mechanical property changes. Therefore, there is a need to raise the recrystallization temperature of tungsten and limit the kinetics of the recrystallization and grain growth processes. In this work, we examine the effect of different types (TiC vs. TaC vs. ZrC) and different concentrations (1.1 vs. 5 vs. 10 wt.%) of dispersed second phase particles in a tungsten matrix on the high temperature performance. The addition of second-phase particles effectively increases the temperature of and time for recrystallization and slow grain growth; however, the addition of a high weight fraction of particles alters the surface chemistry, which may impact subsequent plasma-surface interactions. These results show that the addition of small concentrations of dispersed particles can be effectively employed in tungsten to raise the upper operating temperature limit for tungsten in a fusion reactor.

1. Introduction

Tungsten is the proposed and current plasma-facing material of choice in the divertor region of magnetic confinement nuclear fusion reactors, as it has a high melting temperature, high sputtering threshold, and high thermal conductivity [1]. The operation of a nuclear fusion reactor will expose the plasma-facing materials to high temperatures that can alter their mechanical properties [2]. In the divertor of ITER, materials will be exposed to temperatures in excess of 2000 C, which may cause recrystallization of W. Exposure of W to high temperatures alters the microstructure by causing recrystallization, recovery, and grain growth. These microstructural changes cause degradations in the strength, decrease the fracture toughness, and enhance embrittlement [3,4].

While the recrystallization temperature of W is commonly over 1000 C, the exact temperature can vary based on microstructure and other parameters [4]. For example, the heating rate can affect the recrystallization temperature [5]. The annealing time can also influence the recovery, recrystallization, and grain growth kinetics. Recovery and reduction in the dislocation density may begin at 1200 K, while the grain boundary density decreases and grain size increases have been shown to occur at temperatures above 1700 K, indicating the onsets of recovery, recrystallization, and grain growth in pure W [6]. Long-term, high temperature exposure of W will occur for plasma-facing materials in a high-duty cycle reactor, and W must be operated in a temperature regime that allows for stable microstructure and mechanical performance [7,8].

Attempts have been made to alter the microstructure of tungsten to improve its performance in a fusion reactor environment. Nanocrystalline W has been shown to enhance radiation tolerance but is susceptible to rapid grain growth and recrystallization [9,10]. Substitutional alloys with rhenium allow for an increased recrystallization temperature and increased high temperature strength, but too high of a Re concentration can cause embrittlement [11,12]. Potassium-doped tungsten has been used as filaments due to its high recrystallization temperature of 1600 C and refined microstructure [1]. Potassium-doped W-Re alloys have also displayed enhanced recrystallization resistance [12]. Dispersion strengthened alloys pin grains, which strengthen and inhibit grain growth. Thoria dispersoids, for example, have been shown to raise the recrystallization temperature [1]. Dispersoids stabilize the microstructure and restrict grain boundary movement [1,12]. The impact of these

* Corresponding author at: 104 S. Wright St., Urbana, IL 61801, USA.
E-mail address: ejlang2@illinois.edu (E. Lang).

https://doi.org/10.1016/j.jnucmat.2020.152613
0022-3115/

second phase dispersoids on the resulting microstructure and material chemistry has not been thoroughly examined, however.

Carbide-dispersion strengthened W has been proposed as an alternative to pure W as a PFC, as it has displayed enhanced ductility, crack resistance, and radiation tolerance. Tungsten doped with 0.5 wt.% TaC has displayed recrystallization inhibition up to 1600 C [13,14]. The onset of recrystallization of W-0.5-ZrC specimens is 1300 C [15]. Kurishita, et al. meanwhile showed that the addition of 2.2 and 3.3 wt.% TaC resulted in no microstructure change after annealing at 2000 C, while W-1.1TiC did show a change in W grain size after exposure at 2000 C [16], demonstrating the impact of dispersoid type and concentration on the material performance. Finally, in an analysis of the activation energy for recrystallization of pure W and W-Y_2O_3 alloys, it was found that the yttria-strengthened alloys inhibited recrystallization and had an activation energy greater than that of pure W, attributed to the presence of the yttria particles hindering grain boundary migration [17].

In this work, the impact of dispersoid carbide concentrations and type on limiting recrystallization and mechanical property change through second phase pinning under isochronal annealing from 1200-1800 C and isothermal annealing up to 12 hrs. is demonstrated. The changes in mechanical properties after annealing are studied via Vickers hardness, and microstructural investigations are performed with SEM/EBSD. Additionally, the effect of second phase particle additions on surface and bulk chemistry are analyzed to determine potential impacts on material performance in a fusion environment. We show that a high concentration of fine dispersoids is most effective to be reliably employed as plasma-facing materials in a fusion reactor.

2. Materials and methods

2.1. Materials

Samples used in this study were dispersion-strengthened W specimens were fabricated via spark plasma sintering. The specimens of interest were dispersion-strengthened tungsten alloy samples strengthened with TiC, TaC, or ZrC. Samples were fabricated with 1.1, 5, or 10 wt.% of the added carbide, with the balance being W (the subsequent sample naming convention is: W-10ZrC contained 10 wt.% ZrC, 90 wt.% W). Samples were fabricated via spark plasma sintering, resulting in micron-sized W grains with (0-1 μm-sized) transition metal carbide particles both at grain boundaries and inside W grains. Transition metal oxide phases were also observed on the consolidated specimen surfaces, indicating a chemical breakdown of the starting powders and the ability of the added transition metals to capture impurity oxygen atoms in the W matrix. Additional details about the specimen fabrication and characterization can be found elsewhere [18].

Monolithic, ITER-grade W purchased from Sumitomo Electric Co. specimens were used as a control in this study. All specimens were polished to 0.05 μm diamond suspension prior to experimentation.

2.2. Annealings

Isochronal annealings were performed in a W element furnace in an Ar atmosphere. Specimens were placed in a Ta box during annealing to prevent contamination of the surface. Annealings were performed for 60 minutes at 1200-1800 C with a ramp rate of 20 C/min with a furnace cooling.

Isothermal annealing at 1350°C was performed using an effusion cell. Prior to annealing, samples were ultrasonically cleaned with acetone and rinsed with isopropyl alcohol and then placed in a Al_2O_3 crucible. The instrument reached a base pressure of $< 10^{-6}$ Pa prior to initiating the annealing program. The effusion cell was heated by W filaments and the surrounding structures were water cooled and shielded with Ta foil prevent outgassing. The samples were heated in three stages. We first used an annealing rate of 8.8 C/min. up to 1000 C. The heating ramp was then paused for 30 min. at that point to allow for outgassing of any remaining chemisorbed species. Following this step, annealing resumed with a slower heating rate of 17.5 C/min. until the samples reached 1350 C. Specimens were then held at temperature for 2, 4, 6, 8, or 12 hours.

2.3. Specimen analysis

Vickers hardness was performed before and after heating with a 200g load at 20 s dwell time. Five indents were performed at various locations on the specimen surfaces. The average of the 7 indents was taken, and the error represents the standard deviation of these indents.

Electron microscopy was performed using a JEOL 7000F SEM. Additionally, a Scios 2 FIB was used, and EDAX EBSD and JEOL 7000F with HKL EBSD software. EBSD mappings were acquired with a 30 kV beam and collected using a Hikari Super EBSD detector. Mappings were done sub-micron step sizes on the chosen areas. Data was slightly filtered with EBSD processing software (HKL Tango or EDAX Team) to improve pattern quality as as-annealed surfaces had some surface roughness that impacted pattern quality. Grain size estimates were performed from EBSD data and backscatter SEM images using the line intercept method.

Specimen chemistry was investigated via XPS and XRD. A Phillips X'Pert 2 was used for XRD measurements. XPS measurements were performed on the Ion-Gas-Neutral Interaction with Surfaces (IGNIS) facility, an *in-situ* irradiation and surface analysis facility at the University of Illinois, using a Specs XR-50 x-ray source (Al anode) and Specs Phoibos 150 EP hemispherical energy analyzer.

3. Results and discussion

The influence of annealing temperature on the grain size and hardness is shown in Fig. 1a-f. The pre-annealing, as-fabricated hardness of the pure W (IGW) sample is higher than the 1.1wt.% DS-W specimens due to the higher density. As shown in Table 1, the densities of the 1.1wt.% DS-W specimens is less than that of pure W (~19.3 g cm^{-3}) and a lower density leads to a lower Vickers hardness value. The lower density of the DS-W specimens is attributed to minute, intrinsic porosity from the SPS fabrication process, while the IGW specimen underwent a hot-pressing and cold-rolling process during fabrication, which increases the density and hardness due to increased processing time and introduction of dislocations during the rolling process.

The pure W sample exhibits an apparent increase in grain size and a corresponding drop in hardness after annealing at 1400 C for 1 hr.; thus the recrystallization temperature (T_{RX}) for pure W in this study is between 1200 and 1400 C, which agrees with many other studies of pure W. EBSD maps in Fig. 2a-c show that after annealing at 1800 C, large recrystallized grains have developed.

The DS-W materials exhibit less definitive behavior, as the grain size and hardness changes are a function of the dispersoid type and concentration. The W-ZrC materials show slight grain growth after annealing at 1800 C, but the W grain size is still <10 μm. Correspondingly, there is no drop in hardness from the pre-annealed state. EBSD maps in Fig. 2a shows that the W-1.1ZrC samples still have a fine grain size after annealing at 1800 C, and there is no clear evidence of newly formed, recrystallized grains.

The W-TiC materials all show a drop in hardness after annealing at 1400-1600 C. However, only the W-1.1TiC sample exhibits an increase in grain size, while the W-10TiC and W-5TiC specimens

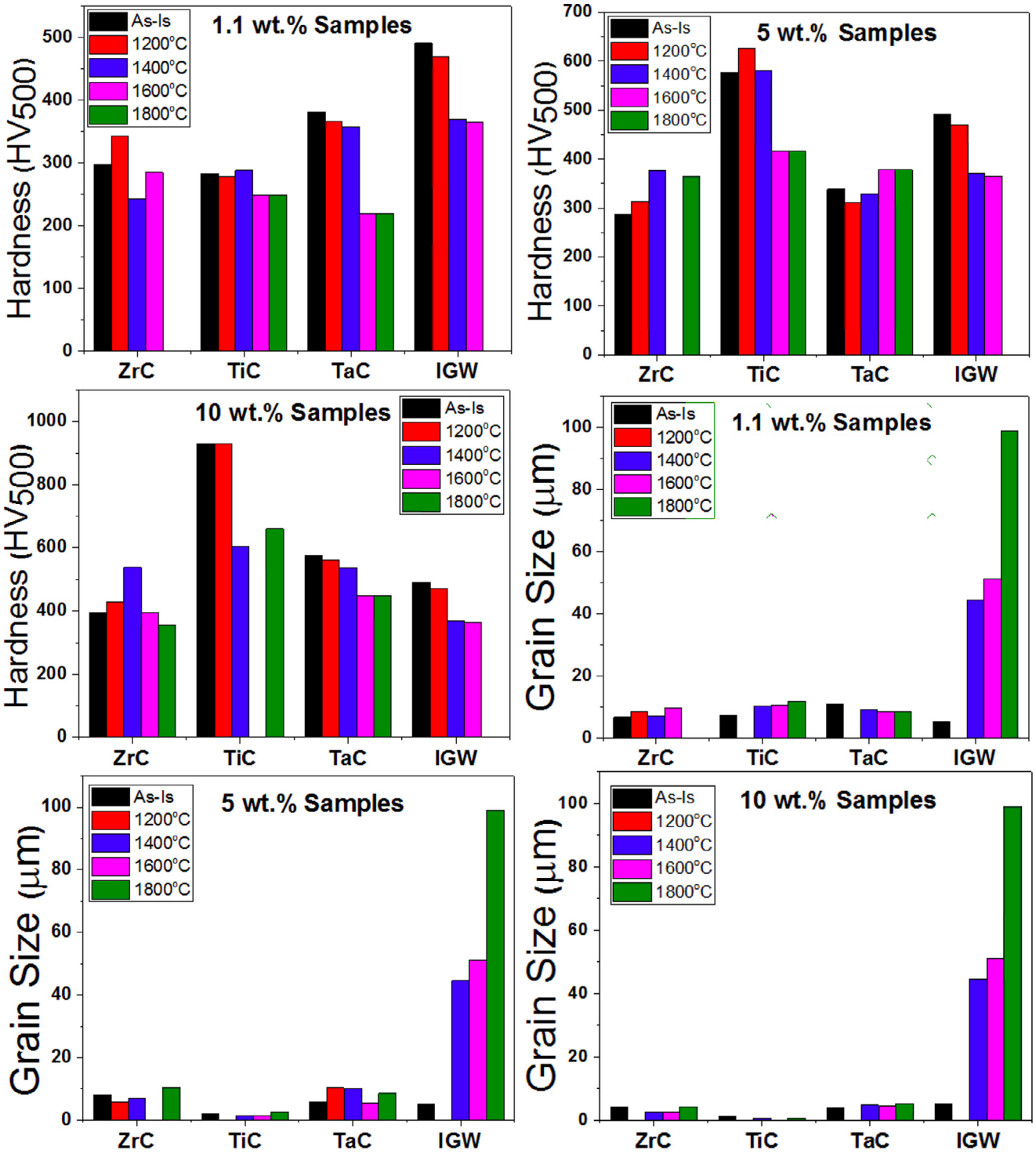

Fig. 1. a-g: Change in hardness as function of annealing temperature for **(a)** 1.1wt.% samples, **(b)** 5wt.% samples, and **(c)** 10wt.% samples. Change in W grain size as function of annealing temperature for **(e)** 1.1wt.% samples, **(f)** 5wt.% samples, and **(g)** 10wt.% samples.

maintain their micron-sized grains up to 1800 C. SEM investigations showed that the W-1.1TiC samples still have a fine grain size after annealing at 1800 C as shown in Fig. 1d, and there is no clear evidence of newly formed, recrystallized grains.

Similarly, the W-TaC specimens show a drop in hardness at ~1600 C, but no samples show an increase in the average grain size. EBSD maps in Fig. 2c of the W-1.1TaC sample show no evidence of new grain formation or grain growth after annealing at 1800 C. The fine grain size of the W-1.1TiC and its maintenance after high temperature exposure is attributed to the fine, intragranular dispersoids shown in the micrographs of an as-fabricated specimen in Fig. 3. The fine dispersoids both at W grain boundaries and within W grains can prevent dislocation motion during the initial recovery stages, and prevent grain boundary motion during recrystallization and grain growth.

The drop in hardness without an increase in grain size may be attributed to the growth of surface pores. Pores inhibit recrystallization and inhibit grain growth, but surface pores would

Table 1
Parameters of consideration for particle stimulated nucleation: Specimen density [18], average size of the W grains (R) and dispersoids (d), the volume fraction of dispersoids (F_v), the ratio of particle volume fraction to size (F_v/r), the dispersoids per grain $N_g = {}^{8F_vR^3}/_{d^3}$, and the grain size following recrystallization as predicted by Zener pinning $X = dF_v^{-1/3}$.

Sample	Density (g cm^{-3})	W Grain Radius (μm)	Dispersoid Radius (μm)	Dispersoid Volume Fraction (F_v)	N_g	Predicted Grain Size X (μm)
1.1ZrC	17.5	3.35	0.875	0.0283	1.5811	55.2
5ZrC	16.9	4.09	1.12	0.1317	6.3901	4.4
10ZrC	17.2	2.07	1.14	0.2425	1.4413	3.6
1.1TiC	17.2	3.70	1.085	0.0402	1.5942	42.9
5TiC	17.2	1.04	0.265	0.1717	10.3784	0.9
10TiC	14.9	0.54	0.3	0.3044	1.7264	0.9
1.1TaC	17.4	5.44	1.11	0.0145	1.7021	174.9
5TaC	17.1	2.91	0.975	0.065	1.7281	4.8
10TaC	16.9	1.84	0.84	0.1281	1.3464	3.3

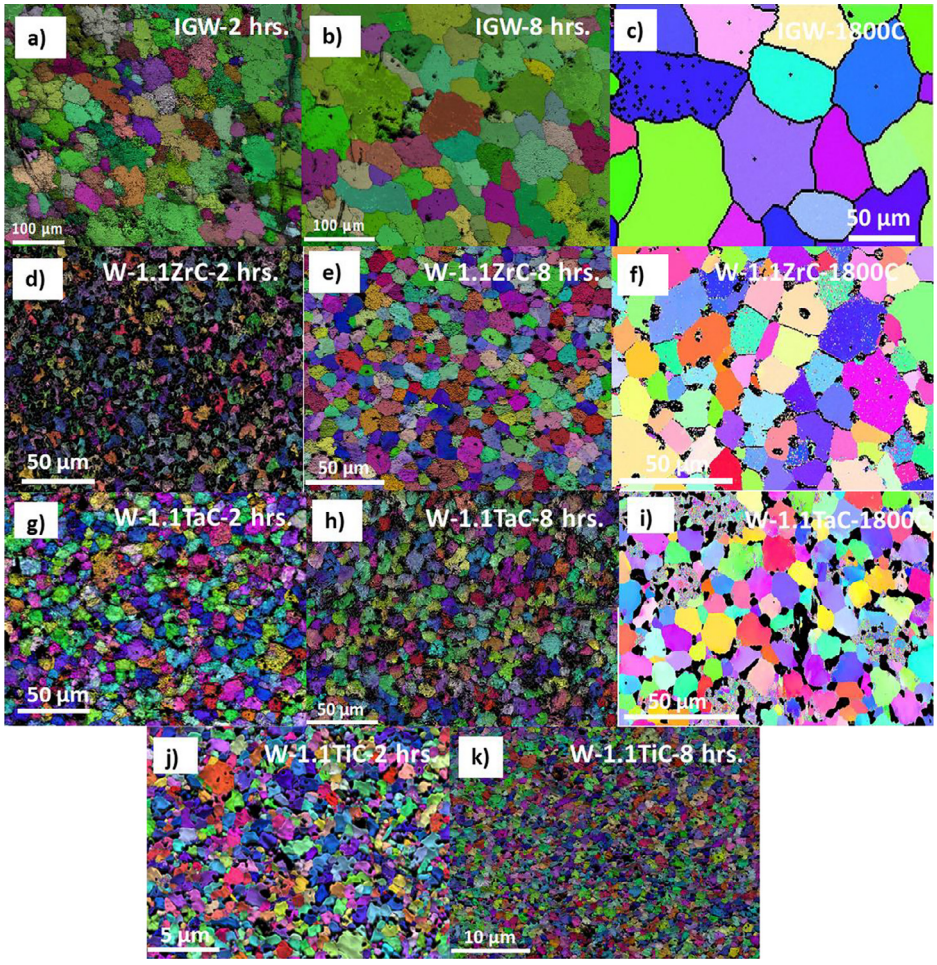

Fig. 2. a-h: EBSD maps of samples annealed at indicated conditions: **(a)** IGW_2hr., **(b)** IGW_8hr., **(c)** IGW_1800, **(d)** W-1.1ZrC_2hr., **(e)** W-1.1ZrC_8hr., **(f)** W-1.1ZrC_1800, **(g)** W-1.1TaC_2hr., **(h)** W-1.1TaC_8hr., **(i)** W-1.1TaC_1800, **(j)** W-1.1TiC_2hr., and **(k)** W-1.1TiC_8hr. Results show that the pure W sample underwent grain growth after annealing at 1800 C for 1 hr., and 1350 C for 8 hr. while the 1.1wt.% alloys show no grain growth after annealing at 1800 C for 1 hr. or at 1350 C for 8 hrs.

contribute to decreased hardness values. The presence of oxygen within Mo-TiC samples has been shown to promote pore formation that contributes to a drop in the hardness [19]. The pores, while contributing to the drop in hardness, can also explain the lack of change in grainsize, as pores have been shown to have a significant Zener pinning effect to prevent grain growth [19, 20].

Another factor in the hardness values is the development of surface oxides. Surface oxide growth was observed on all 10wt.% samples, as shown in Fig. 4a-b. The white regions on the surface show that surface oxides grow primarily in the dispersoids regions. XPS investigations, not shown, of the 10wt.% samples after annealing indicate the formation of W oxide and confirm an increase in the oxide concentration and an alteration to the Ti/Zr oxidation states. Additionally, XRD investigations showed the presence of metal oxides. When the sample is cross-sectionally imaged in the SEM-FIB, no alteration to the sub-surface dispersoid size or distribution is observed, therefore the oxidation of dispersoids is likely limited to those on the surface. These metal oxides indicate that the surface composition may not be stable under high temperature exposure, even if the grain size and mechanical properties are maintained.

Finally, the drop in hardness without grain growth may simply be attributed to the fact that the alloys are still in the recovery regime and have not yet transitioned to the grain growth regime

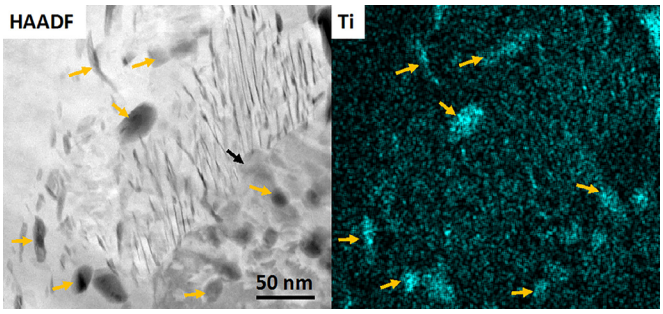

Fig. 3. HAADF-STEM and corresponding STEM-EDS micrographs of as-fabricated W-1.1TiC specimen showing 10 nm-sized Ti dispersoids (yellow arrows) dispersed within W grains, as W grain boundary denoted with black arrow. EDS mapping generated with a 3 × 3 pixel averaging kernel.

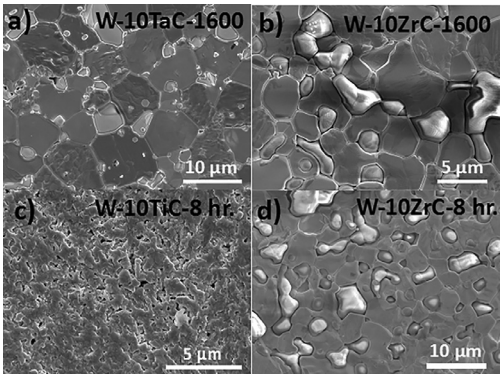

Fig. 4. a-d: SEM micrographs of **(a)** W-10TaC_1600, **(b)** W-10ZrC_1600, **(c)** W-10TiC_8hr., and **(d)** W-10ZrC_8hr. samples showing oxide growth (white) on the surface after annealing.

that occurs following recrystallization. Therefore, this would mean that dislocation motion and rearrangement is reducing the mechanical strength, but there is not yet nucleation and growth of dislocation-free grains. Therefore, the recrystallization kinetics are likely delayed in the DS-W materials. Indeed, grain growth will only occur after recrystallization (formation of new grains) is complete. Therefore, it is likely that the times and temperatures examined here were not sufficient to complete the grain formation process to proceed towards grain growth. Thus, to fully complete the recrystallization process and being grain growth, temperatures greater than 1800 C are needed for the W alloys. To further investigate the kinetics of the recovery, recrystallization, and grain growth processes, isothermal annealing at 1350 C were carried out for between 2-12 hrs.

The changes in hardness after annealing at 1350 C for different times are shown in Fig. 5a-b for specimens, as indicated in the figure. The pure W sample shows a significant drop in hardness after annealing for 2 hrs., mirroring the recrystallization observed after 1 hr. exposure at 1600 C. Further annealing up to 8 hrs. resulted in significant grain growth as shown in EBSD maps in Fig. 2g-h, but no more drop in hardness, indicating that recrystallization was complete after ~4 hrs. exposure, after which grain growth began. A fully recrystallized, altered microstructure is observed after 8 hrs. exposure.

Results show that the 10wt.% alloys show similar drops in hardness as pure W, although the time required to reach minimum hardness is longer than pure W. This shows that these materials require a longer time to the recrystallization process to proceed, as the dispersoids may be slowing the recrystallization kinetics as compared to pure W. However, the SEM micrograph in Fig. 4c-d shows that the W grain size is unchanged, indicating that the grain growth phase was still not yet reached after annealing for 12 hrs. Additionally, Fig. 4c-d shows that the 10wt.% materials developed surface oxides (white in the micrographs), both within the W grains and dispersoids. Again, this indicates chemical instability of the surface that may not be tolerable for a plasma-facing material in a fusion reactor.

The W-10TiC and W-10TaC samples when annealed for 1 hr. show a drop in hardness at ~1400 C, but no change in grain size. Similarly, annealing at 1350 C shows a drop in hardness after ~2-4 hrs. but no change in grain size. The high concentration of dispersoids may be offering many nucleation sites for sub-grain formation, reducing the hardness without yet crystallizing into grains.

The 1.1wt.% samples, conversely, show no oxide growth and also very little change in hardness after annealing for 12 hrs., as shown in Fig. 5b. Additionally, no grain growth is observed in the EBSD maps shown in Fig. 2d-f even after annealing for 8 hrs. The black regions in the EBSD maps are either pores or second phase dispersoids that were unindexable by the EBSD software. These results show that the 1.1wt.% materials slow the recrystallization and grain growth kinetics compared to pure W, and do so without the development of potentially detrimental surface oxide growth.

The higher recrystallization temperature of the DS-W materials as compared to pure W agrees with other studies examining the recrystallization behavior of W alloys. Z.M Xie, et al. determined that the recrystallization temperature of W-0.5ZrC alloys was ~1300 C [15]. The W-ZrC alloys of similar composition (1.1 and 0.5 wt.%) studied here do not exhibit recrystallization at 1300 C, instead of maintaining their grain size and hardness up to 1800 C. Similarly, X. Zan, et al. showed that the recrystallization kinetics of W are slowed by the inclusion of 2% Y_2O_3 in the W matrix. Annealing at 1350 C, the time required for half-recrystallization of W-2%Y_2O_3 was ~6 hrs. compared to ~1 hr. for pure W [17].

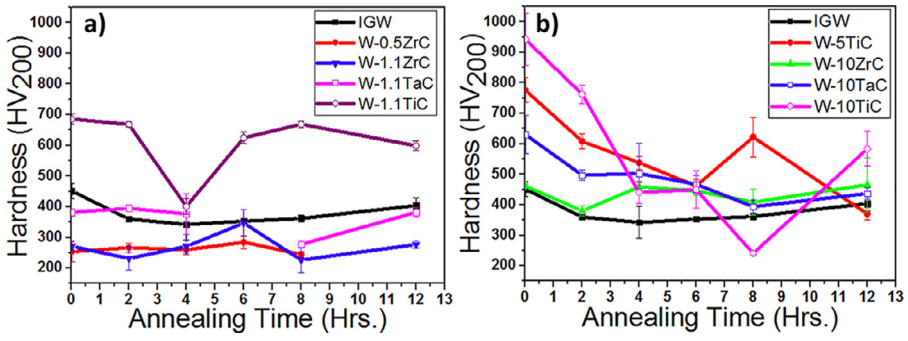

Fig. 5. a-b: Change in hardness as a function of annealing time at 1350 C for samples, as indicated. Drop in hardness of Pure W and 10wt.% samples show evidence of recrystallization, while 1.1wt.% samples show no drop in hardness.

The second phase particles exert a pinning force that counteracts the driving force for growth. When the grain size is smaller than the average particle spacing, the grains will not be pinned and can grow freely. However, if there is a sufficiently high number of particles per grain N_G then grain growth can be suppressed. If $N_g = {}^{8F_vR^3}/_{d^3}$ then grain growth is controlled. However, second phase particles >1μm in size can provide nucleation sites for recrystallization. For the alloys studied here, the average dispersoid size, W grain size, dispersoid volume fraction, and calculated N_G values are given in Table 1. From these values, it is clear that all alloys have $N_G \geq 1$, which can effectively suppress W grain growth [20].

For materials with a large fraction of second phase particles, a limiting grain size will be reached when the driving pressure equals the Zener pinning pressure. Zener pinning occurs when the pressure on a boundary due to pinning by particles equals the driving force for growth. Based on the W grain size and dispersoid volume fraction, estimates for the Zener limited grain size can be calculated to be $X = dF_v^{-1/3}$ [20]. The Zener limited grain sizes are also given in Table 1 and indicate that the measured grain sizes for the 5 and 10wt.% samples are roughly the same as the predicted Zener-limited grain sizes. Thus, these concentrations of dispersoids should not have any more change in grain size, even if the temperature or annealing time was increased further. This may indicate that the 10wt.% samples have undergone recrystallization and grain growth via Particle-Stimulated Nucleation, yet the Zener-limited grain size is very similar to the initial grain size, so no significant change in the W grain size is being observed.

The 1.1wt.% samples, however, have Zener limited grain sizes that are much greater than the final grain sizes measured in these experiments. Thus, it is assumed that the Zener limit has not been reached, and further annealing may result in grain growth or a broadening in the grain size distribution. The 1.1wt.% samples thus experience delayed recrystallization, and not new grains are not yet nucleated and growing as higher temperatures or longer annealing times are needed to drive full recrystallization and grain growth.

The effect of the type of second phase added is more difficult to decipher and is tied to the second phase concentration. The above discussion showed that the 1.1wt.% DS-W specimens show the most promise for inhibiting recrystallization and preserving microstructures after high temperature exposure. Within this subset of materials, the W-1.1TiC specimens are the most attractive primarily for their presence of fine (<100 nm diameter) dispersoids, as the W-1.1ZrC and W-1.1TaC specimens do not show similar dispersoids within the W matrix. The W-1.1TiC specimens limit W grain size growth and hardness drop to longer times than the W-1.1TaC and W-1.1ZrC specimens. The base temperature of ~1000 C of a fusion PFC material and long necessary exposure and operational times motivates the need to have a material that can withstand those temperatures for long times, which the W-1.1TiC specimen did most effectively. Therefore, future studies focusing on the W-1.1TiC materials would be of most relevance.

These results show that the ability to control the dispersoid size has an impact on the recrystallization response. Controlling the size of dispersoids to <~100 nm can provide an avenue for best control of the microstructure. Limiting the dispersoid concentration to 1.1wt.% provides the best route for limiting the dispersoid size. Therefore, this result, combined with the stable surface composition indicates that this composition should be the subject of most future work.

Prior work on DS-W materials examined their ability to alter the W microstructure and subsequently alter the irradiation tolerance, to improve PFC performance under He bombardment. Pure W has been shown to have an altered response to He irradiation after recrystallization. Therefore, it is desirable for PFC materials to have a predictable and consistent response to He irradiation, which may be achieved through having a consistent microstructure. Therefore, the ability of DS-W materials to preserve their microstructure after high temperature exposure indicates they may preserve their response to He irradiation. These studies show that the DS-W materials do indeed preserve the starting microstructure and therefore would maintain their response to He bombardment after high temperature exposure.

Therefore, the addition of 1.1wt.% ZrC/TaC/TiC effectively suppresses recrystallization and grain growth in W by delaying the recrystallization kinetics. Additions of 10wt.% result in significant surface oxide growth, which would be detrimental to material performance, and plasma performance if used as a plasma-facing material in a fusion reactor environment.

4. Conclusions

The ability to raise the recrystallization temperature and delay the grain growth kinetics of tungsten can significantly impact the performance of tungsten-based materials in a nuclear fusion reactor environment. In this work, dispersion-strengthened tungsten, W micro-alloyed with TiC, TaC, or ZrC, has been shown to effectively raise the recrystallization temperature and delay grain growth as compared to pure W. The dispersed second phase particles effectively pin W grains to limit their growth under a series of annealing conditions. Most significantly, the presence of intra-granular fine (~10 nm diameter) dispersoids within W grains show the most promise to maintain a stable microstructure, while also potentially providing beneficial radiation tolerance in a fusion radiation environment [21]. The addition of a high concentration of second phase particles, however, while effectively pinning W grains, results in the formation of surface oxide particles, which may impact the material performance under irradiation. This work motivates further studies on the subsequent irradiation performance of dispersion-strengthened W after heat treatment.

Declaration of Competing Interest

The authors declare that they have no known competing financial interests or personal relationships that could have appeared to influence the work reported in this paper.

CRediT authorship contribution statement

E. Lang: Conceptualization, Data curation, Formal analysis, Investigation, Methodology, Writing - original draft. **H. Schamis:** Data curation, Formal analysis, Writing - review & editing. **N. Madden:** Data curation, Formal analysis, Writing - review & editing. **C. Smith:** Data curation, Formal analysis, Writing - review & editing. **R. Kolasinski:** Data curation, Resources, Formal analysis, Writing - review & editing. **J. Krogstad:** Project administration, Supervision, Writing - review & editing. **J.P. Allain:** Funding acquisition, Project administration, Supervision, Writing - review & editing.

Acknowledgments

The characterization was carried out in part in the Frederick Seitz Materials Research Laboratory Central Research Facilities, University of Illinois. This work is supported by US DOE Contract No. DE- SC0014267. Sandia National Laboratories is a multimission laboratory managed and operated by National Technology and Engineering Solutions of Sandia LLC, a wholly owned subsidiary

of Honeywell International Inc. for the U.S. Department of Energy's National Nuclear Security Administration under contract DE-NA0003525.

References

[1] E. Lassner, W.D. Schubert, Tungsten, Plenum Publishers, 1999.
[2] J. Linke, et al., Matter Radiat. Extremes 4 (2019) 056201.
[3] A. Hasegawa, et al., Journal of Nuclear Materials 471 (2016) 175–183.
[4] K. Farrell, et al., Journal of Less-Common Metals 13 (1967) 141–155.
[5] C.M. Denissen, et al., International Journal of Refractory Metals and Hard Materials 24 (2006) 321–324.
[6] A. Manhard, et al., Pract. Metallogr. 52 (8) (2015) 437–466.
[7] A. Alfonso, et al., Journal of Nuclear Materials 455 (2014) 591–594.
[8] A. Alfonso, et al., Fusion Engineering and Design (2015) 1924–1928 98–99.
[9] O. El-Atwani, et al., Nuclear Fusion 54 (2014) 083013 (9pp).
[10] A. Suslova, et al., Scientific Reports 4 (2014) 6845, doi:10.1038/srep06845.
[11] Y. Mutoh, et al., Journal of Materials Science 30 (1995) 770–775.
[12] K. Tsuchida, et al., Nuclear Materials and Energy 15 (2018) 158–163.
[13] S. Miao, et al., Materials Science and Engineering A 671 (2016) 87–95.
[14] S. Miao, et al., Nuclear Materials and Energy 13 (2017) 12–20.
[15] Z.M. Xie, et al., Journal of Nuclear Materials 496 (2017) 41–53.
[16] H. Kurishita, et al., Physica Scripta T159 (2014) 014032 (7pp).
[17] X. Zan, et al., Fusion Engineering and Design 144 (2019) 1–5.
[18] E. Lang, et al., International Journal of Refractory Metals and Hard Materials 75 (2018) 279–286.
[19] M.K. Yoo, et al., International Journal of Refractory Metals and Hard Materials 14 (1996) 355–364.
[20] J. Humphreys, M. Hatherly, J. Humphreys, G.S. Rohrer, A. Rollett, Phenomena, Recrystallization and Related Annealing Eds., Third Edition, Elsevier, Oxford, 2017.
[21] E. Lang, et al. To be published, 2020.